Journal of Renewable and Sustainable Energy

The development of a screen valve for reciprocating heat pump/engine applications

Cite as: J. Renewable Sustainable Energy **12**, 054101 (2020); https://doi.org/10.1063/5.0007960
Submitted: 18 March 2020 . Accepted: 03 September 2020 . Published Online: 21 September 2020

Muhammad Tahir Ameen, Andrew Smallbone, Anthony Paul Roskilly, and Edward Carpenter

Journal of Renewable and Sustainable Energy ARTICLE scitation.org/journal/rse

The development of a screen valve for reciprocating heat pump/engine applications

Cite as: J. Renewable Sustainable Energy **12**, 054101 (2020); doi: 10.1063/5.0007960
Submitted: 18 March 2020 · Accepted: 3 September 2020 ·
Published Online: 21 September 2020

View Online Export Citation CrossMark

Muhammad Tahir Ameen,[1] Andrew Smallbone,[2,a)] Anthony Paul Roskilly,[2] and Edward Carpenter[3]

AFFILIATIONS

[1]Newcastle University, Newcastle-upon-Tyne, UK
[2]Durham University, Durham, UK
[3]Isentropic Ltd, Fareham, UK

[a)]Author to whom correspondence should be addressed: andrew.smallbone@durham.ac.uk

ABSTRACT

A novel screen valve with rectilinear ports is presented for use in advanced high-efficiency compressors, expanders, heat pumps, or engines. The novel design aims to minimize the pumping losses generated as the working gas flows through the valve by maximizing the effective opening cross-sectional area. In this work, various screen valve configurations have been investigated through a series of experimental tests conducted on a heavily modified research engine for high-speed, high-pressure valve testing. The valves were designed and tested to operate efficiently at both low and high engine speeds ranging between 1500 and 3000 rpm. The valve dynamics were optimized to meet two high-level criteria for performance—namely (1) high speed metrics quantified by its percentage of "maximum dynamic pressure" and (2) low speed metrics quantified by the valve "minimum closure angle." The valves were tested to meet the objective of avoiding any friction-locking issues associated with the valve retainer design. Multiple tests were carried out in pursuit of attaining an improved design. The work concluded that by including a carrier frame (rather than a retainer frame) and upstands on the valve seat, the valve performance was improved significantly. The best design yielded results of 50.4% of maximum dynamic pressure and 25.1° as the minimum closure angle.

NOMENCLATURE

A	Area, m^2
d	Displacement volume, cm^3
D	Cylinder, or piston bore, m
l	Con-rod length, m
P	Pressure, bar
q	Dynamic pressure, kPa
r	Crank radius, m
s	Linear translation of piston, m
S	Stroke length, m
t	Time, s
T	Temperature, °C
v	Velocity, m s^{-1}

Greek letters

θ	Crank angle, °
ρ	Fluid density, kg m^{-3}
σ	Valve porosity, (–)
ω	Rotational speed, rad s^{-1}

Subscripts

c	Closure
e	Effective
p	Piston

Abbreviations

aTDC	After top dead center, °
BDC	Bottom dead center
HS	High speed
LS	Low speed
PHES	Pumped heat energy storage
TDC	Top dead center

I. INTRODUCTION

A. Background

Sliding valves offer strong potential to improve the performance of internal combustion engines and heat pump applications by overcoming some of the inherent shortcomings associated with poppet

valves. These include pumping losses, parasitic losses (associated with moving the valve), and accurate valve opening timing control. Each directly reduces the overall system efficiency. As such, over the decades, there have been numerous patents[1–5] which have included designs for "slide type" valve technologies. However, to date, in compressor, expander, heat pump, or engine applications, these solutions have yet to be realized as the principal means to regulate fluid flow into and out of the working chamber.

A comprehensive literature review has identified that there is very little published research work around this topic; hence this work proposes a new realization of the slide valve. Nevertheless, there are a few patents which suggest alternative valve designs. Slide valves were employed widely for steam engines from at least 1820. The famous "Stephenson's Rocket" (1829) is a very good example. In the early 20th century, slide valves were also configured for combustion engines, such as those described in various patents in Refs. 5 and 6. From a review of past studies,[1,3,4,6] slide valves are shown to present a useful alternative to conventional poppet, reed, and plate type valves, provided they can prove to be sufficiently simple and durable.

Therefore, in the current study, an improved design of a slide type "screen valve" is proposed based on the progress from an earlier version, which was first used but not disclosed in the development of a second generation design of a novel reverse Joule–Brayton cycle heat pump.[7] Various valve designs are tested using a bespoke test rig designed to reproduce the operating characteristics experienced in a larger scale (150 kW) reversible heat pump description, which can be found in Refs. 8 and 9. Nevertheless, the proposed valve could also be applied to minimize power losses and increase efficiency of all other common reciprocating machines (compressors, expanders, internal combustion engines, heat pumps, etc.). The following Secs. I B and I C provide an overview of advantages and challenges with regard to earlier forms of valves and highlight the novel features of the proposed valve.

B. Valve types and challenges

There are a variety of historic and currently employed valve types and designs used in positive displacement machines. In broader terms, they can be categorized as slide and non-slide valves. Slide valves, which were first used in steam locomotives, operate with a movement in the plane of the port to cover or uncover it. Non-slide valves, such as the poppet valve, operate by a lifting action from the seat with a movement perpendicular to the plane of the port. Other prominent examples of non-slide valves include reed and plate valves. These are commonly applied in two-stroke engines, reciprocating compressors for domestic and industrial refrigeration systems, and gas processing industries.[10–19] Poppet valves remain the main type of valve used today in internal combustion engines for intake/exhaust flow control.[16,20–22] (Fig. 1 shows examples of different valve types.) The choice and operation of the valve technology are fundamental to unlocking higher thermodynamic efficiencies and the overall performance of reciprocating machines, as they underpin key loss mechanisms for any suction and discharge process.[23] Many research teams have developed competent designs for specific applications, with the aim of improving valve timing, and actuation mechanisms. Their results show that the performance of any reciprocating machine is critically linked to the mechanism, accuracy of the valve timing, and dynamic operation of the valve.[24] In reciprocating compressors, reed and plate valves are

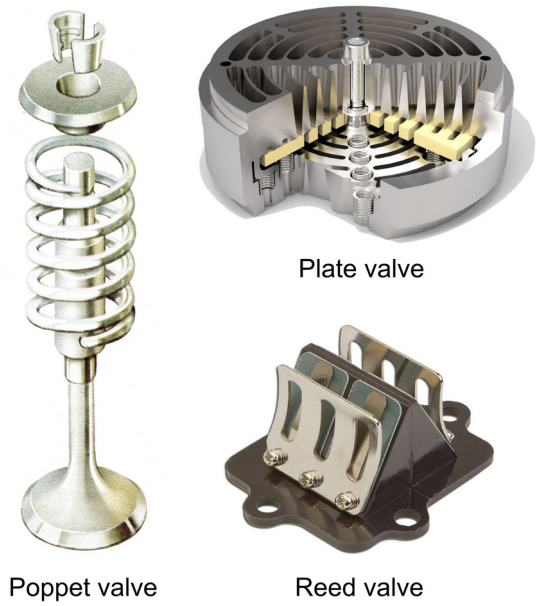

FIG. 1. Various valve types used in reciprocating engines and compressors.[26–28]

reported to be the main cause of recurring maintenance shutdowns. Valve failure and leakages have led to hazardous component failure and thus to increased operational costs. Developments by Brun *et al.*,[23] used a finite element model to validate the results against experimental test data for plate transient stress analysis and a numerical analysis tool was presented to predict the ongoing valve performance. Pichler *et al.*[10] and Wang *et al.*[13] identified the methods to accurately diagnose the valve failure event in compressors. Silva *et al.*[12] presented a model which aimed to predict gas leakage caused by incomplete sealing of reed valves. Ma *et al.*[25] presented a succinct review of past studies conducted to improve the dynamics of reed and spring-loaded valves. The work mainly focused on varying design parameters to investigate the dynamic behavior of a discharge reed valve in reciprocating compressors.

In addition, patents[1–4] have been primarily published by automotive engine developers who identified the opportunities and challenges of poppet and slide valves. It is known that there are several drawbacks in using poppet valves, such as the valve protruding into the displaced volume thereby risking a damaging impact (thus limiting the range of potential valve timings and lift). A high stiffness spring is known to yield higher engine auxiliary losses as additional engine power must be consumed in operating the valve. Furthermore, the flow of the working fluid is disrupted (causing heat exchange and pressure drop) when an incoming flow makes contact with the head of the poppet valve. Further research[20] has addressed the challenge of piston and poppet valve collision by incorporating a solenoid-operated stepping valve in place of the poppet valve, a solution which yielded a more fuel efficient engine.

Compared to poppet valves, slide valves maximize the available space, thus minimizing the restriction (throttling) as the fluid flows across the cylinder. They have lower mass, low inertia, and perform under reduced mechanical loads.[2,3] It can be concluded that slide

valves offer a potentially simpler layout and therefore present a better alternative.

C. Proposed screen valve

This study presents an innovative valve design which principally operates by exhibiting a combined slide and reed valve action. The valve is characterized as screen valve due to a number of rectangular ports on each component (refer Sec. III for more details). The valve differs from other variants with a major difference being that a thin plate (foil) attached with a carrier frame moves to cover, or uncover, the seat ports. The unique design aims to maximize the open area created by a 2D array of rectangular ports on the valve frame, foil, and the seat. The main characteristics of the proposed valve are:

(i) Reduced physical obstruction to gas flow into and out of the cylinder.
(ii) Low pressure loss due to increased porosity.[7]
(iii) Fast valve actuation speed.
(iv) Valve opening controlled by flow dynamics around it; no actuation required.
(v) Less dead space, resulting in the option of higher compression/expansion ratios in compressors and expanders.
(vi) Minimized area for heat exchange.
(vii) Long valve life in unlubricated operation.
(viii) High quality valve sealing without excessive precision.

1. Applications

The unique valve has been tested in context with the application to a full-scale heat pump[7,8] [operating in a pressure range of 1–12 bar (absolute)] but, if further developed to meet specific operational requirements, it can potentially be utilized in a variety of applications such as reciprocating compressors of refrigeration systems, heat pumps, commercial reciprocating air and natural gas compressors, and automotive engines. In addition to these, such valves can be usefully employed in Pumped Heat Energy Storage (PHES) technology[9] (with reciprocating machinery), mainly due to the advantage that with a compact valve assembly it is easy to switch between compressor and expander (charge and discharge) modes quickly in compliance with the storage cycle requirements by rapidly changing the valve timing.[7,29]

2. Previous work on screen valves

To date, no development work on the proposed screen valve has been published and therefore there is an opportunity to investigate and improve the design for practical implementation in a heat pump or engine. In the early stages of the ongoing work, the current design was briefly summarized by one of the authors of the present work[7] in the wider context with PHES technology development. The author also published a patent earlier,[29] which involves an apparatus for use as a heat pump. The main features of the design lie in its compactness as compression, expansion, and heat exchange may take place within a single piston–cylinder assembly. This design is also supported by another patent,[30] which proposed a compact design for an air conditioner. For this solution to work efficiently, a new valve design is required to achieve a more compact assembly. The first implementation of the proposed screen valve in any working machine, therefore, can be traced back from early experiments.[7] This valve serves as the basic (initial baseline) prototype for the current investigation.

In the context of this article, this original work[7] is significant and as such it is discussed, as follows, in more detail. The work aimed to shape practical prototypes for a PHES system by making use of the idea of reversible heat/work conversion.[9] Three prototypes were developed at different scales to assess the performance of a full-scale energy storage system. The first prototype used reed valves and was designed to mitigate valve pressure losses and heat transfer during compression and expansion stages. The results identified that the valve should not open unless the pressure is equalized across the valve, as this would avoid the sudden pressure blow-down events which yield significant losses. In the second prototype, pressure loss was addressed by maximizing the valve open area and carefully timing precise valve opening events close to the pressure equalization across each valve. This was achieved by using a novel screen valve technology (under current research). The third prototype used a pneumatic valve actuation system in place of spring actuation, which improved the performance at high speeds.

Pressure losses were reduced by using such valves, but at high speeds, they proved to have friction-locking issues, resulting in performance deterioration. Motivated by early results, in the ongoing study, the novel screen valve has been modified from its existing basic prototype to reduce friction-locking issues and improve performance at high and low speeds. For conducting valve testing, a screen valve test engine has been recently developed.[8] This test engine provides a platform for valve performance evaluation, so that the valves can be tested under conditions similar to those observed in a full-scale reversible heat pump.

II. METHODOLOGY ADOPTED FOR THE CURRENT WORK

Two performance metrics were devised to evaluate the valve performance based on the operational speed:

(a) high speed (HS) metrics and
(b) low speed (LS) metrics.

It was recommended that a valve that meets both metrics simultaneously can be a better solution for operating successfully in a reciprocating machine. The test engine (detailed in Sec. IV) was operated over a range of speeds to generate data for both HS and LS performances. Various design changes were made to develop an optimal design based on the above-mentioned criteria. For each design modification, the valve performance was evaluated by extracting key data such as time vs voltage curves (recorded via an oscilloscope). For interpretation, these results were post-processed into two measurable criteria of performance with the help of a post-processing tool (written in C language). The code extracts the important features on the voltage traces[33] and associates them with valve events. The results were compared with the previous and forthcoming tests, ultimately resulting in a preferred valve configuration.

III. GEOMETRY AND PRINCIPLE OF OPERATION

The main body of a screen valve is composed of three main components which are:

(i) Frame
(ii) Foil
(iii) Seat

Figure 2 shows different views of the valve assembly. The valve operates by the sliding movement of a carrier type frame attached to an actuator. The foil is attached to the frame on the side facing the valve seat and moves like a reed valve to open or close the ports in the stationary valve seat. The vertical drop/lift of the foil is controlled by a pressure differential across the valve. In test 1, a retainer type frame was used and the valve foil slid independently between the stationary frame and the seat. In the remaining tests (tests 2–9), the retainer frame was replaced by a carrier frame so that the sliding action of the foil was minimized for durable operation (foil acted as a reed therefrom). Figure 3 shows the port pattern of a screen valve foil. The foil has multiple ports of the same size ($3.25 \times 7.24\ mm^2$), spread along its plane with a pitch of $8.00 \times 9.24\ mm^2$. The sealing overlap of the foil is 0.75 mm. The thickness and material for valve components are tabulated in Table I.

IV. TECHNICAL SPECIFICATIONS OF THE TEST ENGINE AND HEAT PUMP

In this section, the technical aspects of the test engine and heat pump are underlined. A full-scale (150 kW) heat pump, investigated in the Refs. 7, 9, and 29, is considered here for reference thermodynamic conditions given in Table II. The heat pump has four valves; two "piston" and two "cylinder head" valves. The performance required of these valves is different because of different pressure and temperature conditions experienced during the intake and exhaust strokes of the compression and expansion cycles. The test engine, therefore, evaluates the performance of a valve which is subjected to extreme conditions, the cylinder head valve of the expander in this case.

Figure 4 represents the basic layout of the testing facility. A 5.5 kW electric motor drives a 392 CC engine (rated power: ∼10 kW at 3600 rpm). The rig piston is directly connected with the engine piston. The working volume is above the rig piston, with the valve being able to seal the upper face of the working volume. As the test engine addresses the cylinder head valve, the valve orientation is as shown in the figure. The space above the valve is maintained at a high pressure (∼8–12 bar) and ambient temperature to match the conditions of the expander inlet (see Table II). The valve area differs from the rig piston area, so that the gas velocity is matched to that expected within the heat pump. The working volume has a dead space (tapering region) so that the fractional rate of change of volume can also be matched. Figure 4 also shows connections to external pressure tanks which buffer the top and bias pressures so that pressures do not vary excessively during the cycle. The important design parameters for the test engine and the reference heat pump are enumerated in Table II.

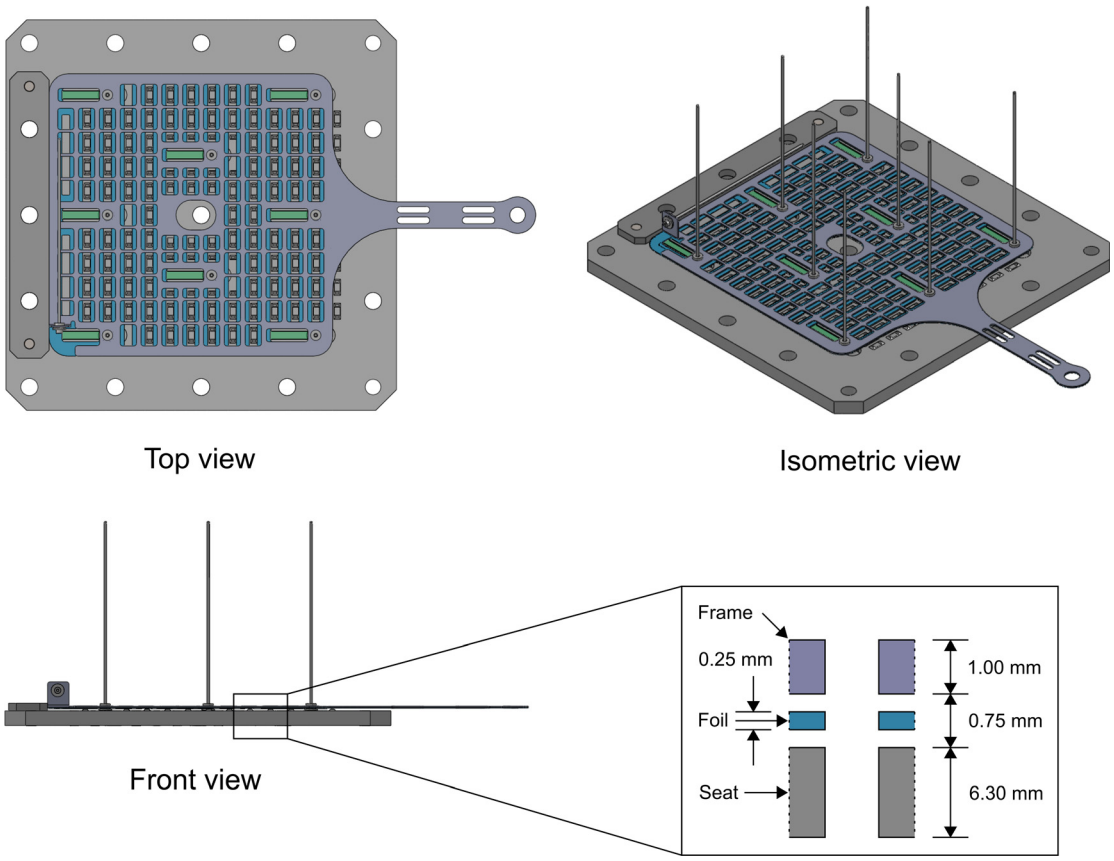

FIG. 2. Different views of the screen valve assembly. A section of front view is enlarged (not to scale) to specify the arrangement of components.

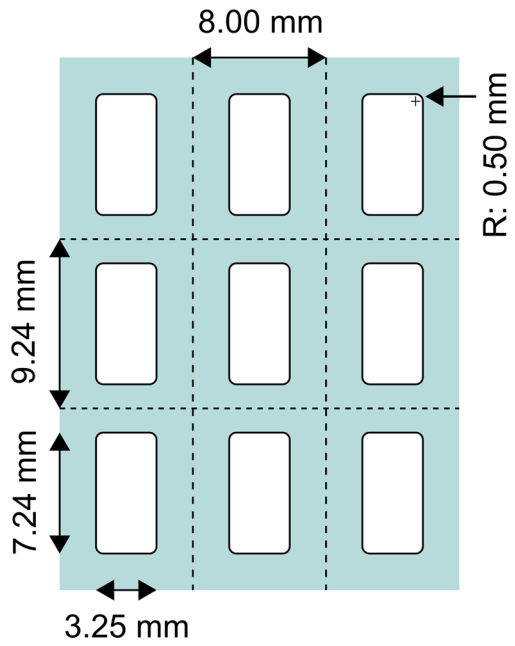

FIG. 3. Valve port design.

TABLE I. Specifications of valve components.

Component	Thickness (mm)	Material
Foil	0.25	Inconel 718
Seat	6.30	Gauge plate BS4659 BO1
Retainer	1.25	Stainless steel AISI 302
Carrier	1.00	Stainless steel (302/304)

Five sensors have been used at specific locations at the rig for data measurement. Two high frequency piezoelectric sensors measure pressures during the cyclic valve motion. One sensor is above the valve in the top pressure space and the other is below the valve in the working space. These sensors generate pulses, which are amplified, and the output is fed to an oscilloscope. Two solid state sensors are used to reflect TDC and cam pulses in the oscilloscope. The TDC sensor is placed near the crankshaft having a toothed wheel mounted on it. The sensor generates a signal when it faces the tooth, indicating that the piston has reached the TDC. Likewise, a signal is displayed on the oscilloscope when the cam triggers the switch, which forces the actuator to move the valve foil from the open to close position. A fiber-optic sensor is used to measure the linear displacement of the valve. With this setup, the oscilloscope displays five time domain signals.

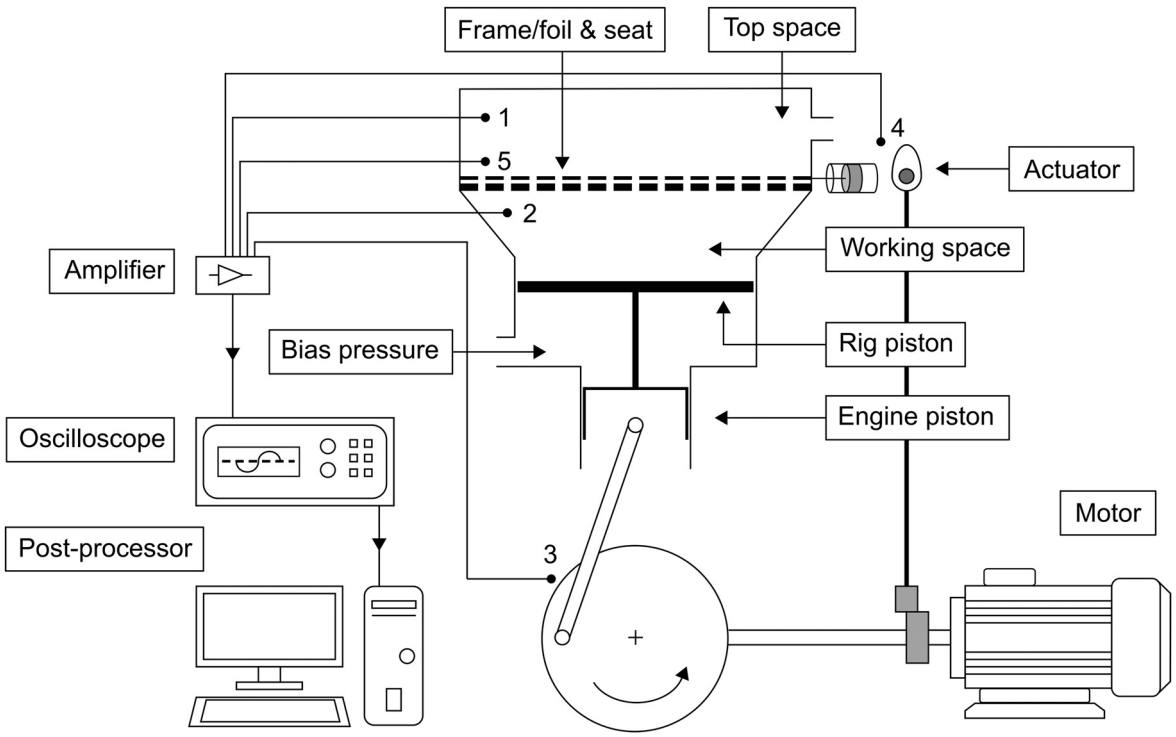

FIG. 4. Schematic representation of the test engine facility. (1) Top space pressure sensor, (2) working space pressure sensor, (3) TDC pulse sensor, (4) valve actuator sensor, and (5) valve displacement sensor.

TABLE II. Design details for the test engine and full-scale heat pump.

Parameters	Test engine	Full-scale heat pump[7]
Effective engine bore, D_e (m)	0.089	0.4
Stroke length, S (m)	0.063	0.1
Con-rod length, l (m)	0.100	0.321
Crank radius, r (m)	0.0315	0.05
Displacement, d (cm^3)	392	12 566.37
Operating speed, N (rpm)	Variable (3000 max.)	250–1000
Effective bore area, A_e (m^2)	15.40×10^{-3} (rig piston)	125.66×10^{-3}
Valve porosity, σ (%)	19.66	20
Valve open area, A_o (m^2)	3.028×10^{-3}	25.132×10^{-3}

V. PERFORMANCE METRICS

To evaluate the valve performance, a new strategy is defined and used in this work. In a heat pump, the valves operate at different speeds depending upon whether they close around mid-stroke or at the end of a stroke. For a valve to be capable of correctly operating at both high and low speeds, it should exhibit good "closing" behavior at both speeds. Hence, the mid-stroke closing performance in the heat pump is evaluated by running the test engine at high speeds, whereas the end-of-stroke closing performance is evaluated by running it at low speeds. Note that defining the valve performance by its closing behavior is due to the fact that valve opening is not directly controlled, as this occurs automatically when pressure equalizes across the valve.

A. High speed metric—% of maximum dynamic pressure (q_{max})

Due to many parameters and constraints being involved, accurate modeling of the valve closure can be quite complex. A simplified method based on dimensional analysis has, therefore, been adopted, which not only reduces the number of experimental variables but also emphasizes the relevant dimensionless variables only. Dimensional analysis suggests that if a system's behavior is dominated by a single non-dimensional number, we can scale between two different systems under consideration.[31,32] In the current situation, the vertical motion of the valve for its closing occurs due to the drag force of the flow. At high speeds, the valve closure is strongly dependent on the increased dynamic pressure (and hence the resulting force). Holding all other non-dimensional numbers constant, we can use this dynamic pressure, q, and the valve porosity, σ, to scale between the test engine and the heat pump. This scaling provides the first performance metric, identified as % of maximum dynamic pressure (q_{max}), and defined by the open port dynamic pressure, q, in the test engine expressed as a percentage of the maximum open port dynamic pressure in the heat pump (q_{max}) operating at 1000 rpm with a compression ratio of 12:1

$$\%\ of\ q_{max} = \frac{\frac{1}{2}\rho v^2|_{\text{test engine}}}{\frac{1}{2}\rho v^2|_{\text{heat pump, max}}} \times 100. \quad (1)$$

As will be shown in Sec. VI, modifications in the valve design yield different values of this percentage. A valve which closes successfully achieving a high "% of q_{max}" is, therefore, required. In Eq. (1), the value of maximum possible open port dynamic pressure for the heat pump under the prescribed conditions is 13.462 kPa (see Appendix A for the calculation procedure).

B. Low speed metrics—minimum closure angle ($\theta_{c,\,min}$)

The closure angle aTDC (after top dead center), which is the crank angle (°) detected at the point of valve sealing, was shown during initial testing to be independent of the machine rotational speed, ω, and thus the fluid speed, v. A simple theory relating the downward force on a valve foil to the dynamic pressure of the passing gas predicts the same result (see Appendix B). The dependence on gas density, ρ, is very weak as $\theta_c \propto \rho^{-1/4}$ [Eq. (B4)] and therefore, for a given operating range of the test engine (8–12 bar, 25–80 °C), any changes can be ignored. It is thus easy to translate this figure, θ_c, to a lost percentage of piston stroke which makes it an especially useful measure of LS performance. Hence, a valve with a low "minimum closure angle ($\theta_{c,min}$)" is sought, which is able to close immediately after the TDC to minimize unwanted expansion prior to the intake stroke.

VI. RESULTS AND DISCUSSION

This section presents the results. Many design changes were brought about, which have been described accordingly in tests 1–9 below. The frame type was the key change, i.e., replacement of the static retainer frame (test 1) by a movable carrier frame (tests 2–9). A Computational Fluid Dynamics (CFD) analysis was also performed prior to using the carrier frame from test 2 onwards. The analysis helped to identify and adjust the development of pressure differentials (and the resulting aerodynamic forces) on the foil at different stages of the operating cycle. Vertical separation of the carrier from the foil was found to be a critical parameter, as was the edge fineness of the carrier ports and carrier overhang of foil elements. Seat geometry was also adjusted during this stage. As a result, the following key changes were applied on the valve design from test 2 onwards.

(i) Addition of upstands on the seat
(ii) Change in the foil spacing
(iii) Insertion of the separation wires and/or foil dimpling
(iv) Foil flexure preloading
(v) Upstand recession

A. Test 1: Screen valve with a retainer frame

To begin with the current testing, a valve similar to that employed in the second and third heat pump prototypes was first used (Sec. I C 2). The valve was a retainer frame type (Fig. 5). As expected, this test also showed poor HS performance, yielding 12.2% of q_{max}. However, the LS performance was remarkable as the test yielded a $\theta_{c,min}$ of 6° aTDC. The reason being that when partially closed, the top surface of the foil is exposed to the full stagnation pressure of the flow and the underside experiences a lower pressure, as the flow separates the foil edges (Fig. 5). The foil is loaded downwards for the entire length of a stroke and therefore seals well at a low speed. The same effect is what limits its HS performance. At a high speed, due to the increased downward force on the foil compared to that at a low speed,

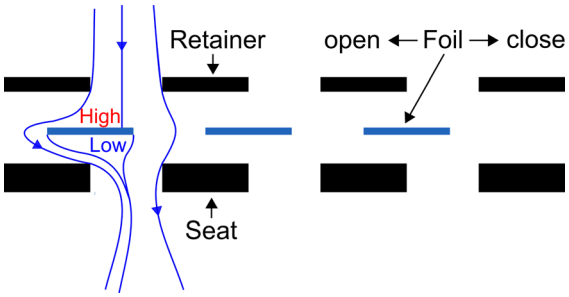

FIG. 5. Test 1. Screen valve with a retainer frame. Separated streamtube is shown at 70% of the stroke.

the valve tends to drop early and becomes friction-locked by the flow in a semi-open position. This test motivated us to develop a new version of frame, i.e., the carrier frame.

B. Test 2: Screen valve with a carrier frame

The carrier is a flat perforated plate which is suspended from a fixed structure via mounting flexures and is allowed to move freely in the lateral direction (perpendicular to the piston motion), whilst it's vertical motion is restricted, as shown in Fig. 6. The foil is attached to the carrier frame by foil flexures. The carrier moves the foil and provides a partial shield from the passing flow. This design improved the HS performance from 12.2% to 29.7% of q_{max}. However, the LS performance declined as the $\theta_{c,\,min}$ increased from 6° to 31.1° aTDC. The improvement in HS performance is due to the reduced pressure between the foil and the carrier during the initial part of the valve motion. This enables the carrier to keep the foil in close proximity until the valve significantly covers the port, after which the increased downward force allows the foil to drop and close the valve. At a low speed, due to the shield provided by the carrier, the foil experiences lesser downward force and, therefore, drops relatively late, consuming more piston stroke.

C. Screen valve with an Mk.1 seat

In the subsequent tests, a new seat design having upstand features (referred in the text as Mk.1) was introduced (Fig. 7). Specifically, if the foil is placed in close proximity to the carrier, the reduced pressure as the flow passes through the carrier ports causes a reduction in pressure in the region between the foil and the carrier, thereby keeping them intact during most parts of the valve motion. As the carrier moves into a position where it fully obstructs the flow, the static pressure above the carrier/foil starts to increase. Ultimately, this pressure increase dominates the low pressure around the carrier port edges and the valve foil drops to the seat. As shown in the figure, the upstands, 0.6 mm high, are machined midway along the framework and have 45° face edges adjoining the plateaux with the seat. This seat was used in the next five tests.

1. Test 3: Reduced foil to plateaux spacing

With a new seat, initially the foil was given a free play of 0.11 mm between the carrier and the plateaux [Fig. 8(a)]. In a HS test, the screen valve sealed, yielding a q_{max} of 54.6%. In terms of fulfilling HS performance metrics, this result was a significant improvement over previous designs. This can be explained by considering the solid interaction between the foil and the upstand, as elaborated in Fig. 17 of Appendix C. A sharp acceleration occurs in the forward direction when the foil slides over the edge of the plateaux (up to about 70% of stroke). In this position, the reaction force from the upstand on the foil now acts at 45° and hence has a component in the forward direction. Because of the central positioning of the upstands, the foil is not only propelled forward, but also guided into the correct closing position. This eventually leads to good HS performance. It is noteworthy that although the HS performance is improved, the foil–upstand nteraction can result in significant wear which is highly undesirable (Sec. VI E).

In a LS test, the $\theta_{c,\,min}$ was found to be 63° aTDC, which is significantly higher than the results with a flat seat design (tests 1 and 2). The reason for such poor behavior is denoted by fairly reduced dynamic pressure conditions at low speeds, thus posing a lack of enough pressure needed to trigger the vertical drop of the foil on the seat. It is noteworthy that this lack of dynamic pressure at low speeds does not pose any threat in the valve without upstand features (test 2), this normally being due to the intrinsic close contact between the foil and the seat.

2. Test 4: Increased foil to plateaux spacing

Optimistic HS performance in test 3 led to an increase in the foil spacing from 0.11 mm to 0.27 mm [Fig. 8(b)]. The valve reached

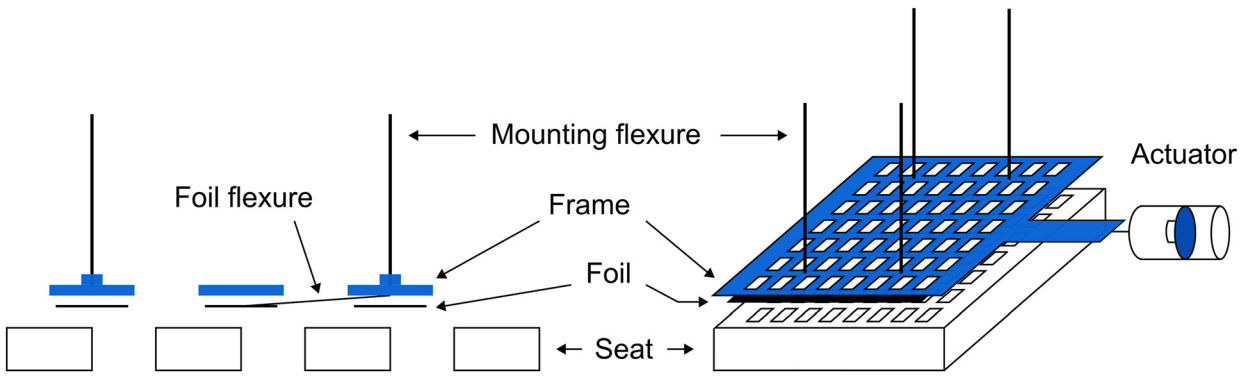

FIG. 6. Test 2. Screen valve with a carrier frame (without subsequent modifications).

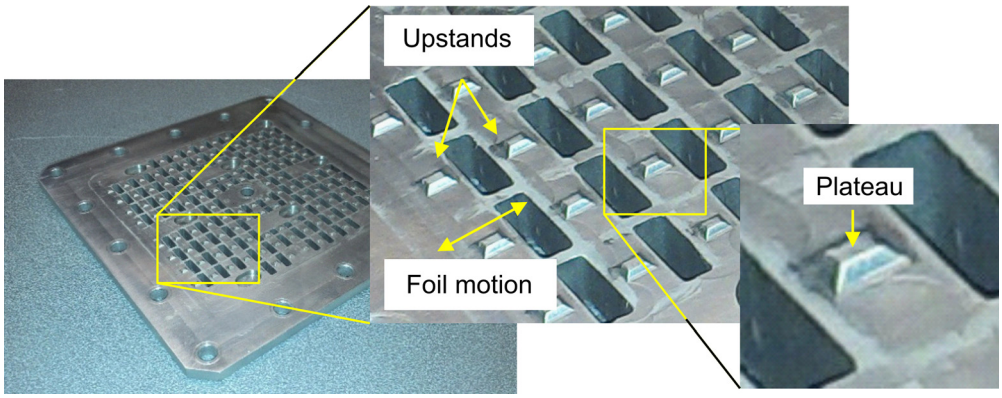

FIG. 7. Mk.1 seat with centrally positioned upstands.

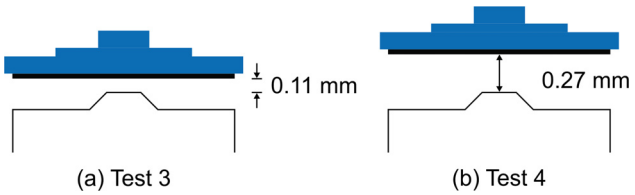

FIG. 8. Tests 3 and 4. Valve configurations.

47.7% of q_{max} in a HS test. However, it performed poorly in a LS test. The recorded $\theta_{c,\,min}$ was 67.9° aTDC. These results depict that increasing the foil spacing decreases both HS and LS performances slightly, the reason being a further decrease in the required pressure (as a result of increased spacing) to trigger the vertical drop of the foil. Having achieved a reasonably better HS performance using a modified seat, the focus at this stage was shifted to explore new means to increase the foil tendency to drop under reduced dynamic pressure conditions.

3. Tests 5–7: Separation wires and/or preloading

In test 5, Ø 0.16 mm wires were inserted between the foil and the carrier plate, as shown in Fig. 9(a). The objective was to place the upper surface of the foil more exposed to the reduced pressure flow around the carrier port edges during down flow conditions, while also allowing pressure to rise in this region as the static pressure above the valve increases on moving to the closed position. A HS test realized 50.9% of q_{max}. Compared to the previous test, this test yielded a much improved LS performance, as the $\theta_{c,min}$ turned out to be 37.8° aTDC. A sudden decline in θ_c from 67.9° to 37.8° is due to the wires which enforce a minimum separation of 0.16 mm between the carrier and the foil. The separation actually prevents any inertial film effects and exposes the foil more to the passing flow. This in turn aids in triggering the vertical drop of the foil to the seat by requiring less dynamic pressure relatively.

The test 5 setup was further modified to include ∼1 mm of downward preload on the foil flexures, as shown in Fig. 9(b). This was achieved by using a wedge tool to plastically bend the flexures, giving them a finite offset from the carrier under zero load. Under the preload, the foil would be lightly held down against the upstand plateaux when in the open position and hence have a greater tendency to drop to the seat when permitted. A HS test reached 50.4% of q_{max}. The change led to a further improved LS performance with a $\theta_{c,min}$ of 25.1° aTDC.

In test 7, the wires were removed but the preload was still applied, as shown in Fig. 9(c). This design yielded 35.3% of q_{max} in a HS test. Compared to the nearly consistent HS performance in the previous four tests (tests 3–6), this decline is attributed to the foil being too far from the carrier to allow the reduced pressure above the foil to hold the two elements together. On the other hand, no significant change to the LS performance was realized, as the valve closed at 22.2° aTDC indicating merely a 2.9° improvement. This suggests that wires offer no sizable benefit if the foil is sufficiently preloaded. The last two designs present an outperforming configuration so far in meeting both performance metrics.

D. Screen valve with an Mk.2 seat

In the next step, a new valve seat, referred to as Mk.2, was developed with a new upstand pattern on the seat. In contrast to the Mk.1

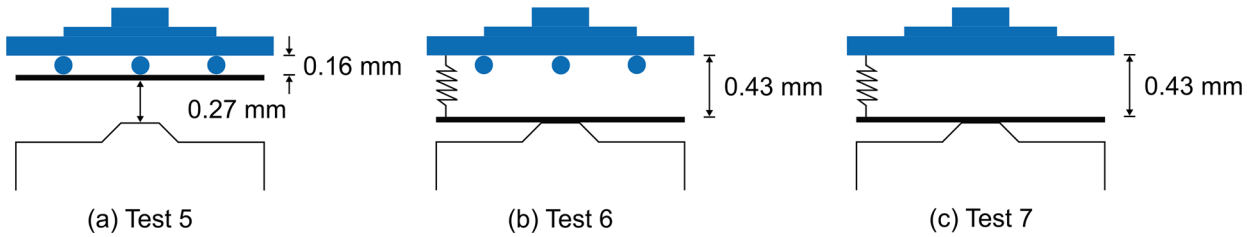

FIG. 9. Tests 5–7. Valve configurations.

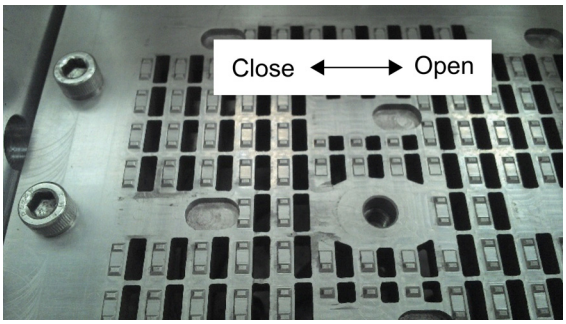

FIG. 10. Mk.2 seat with divided and receded upstands.

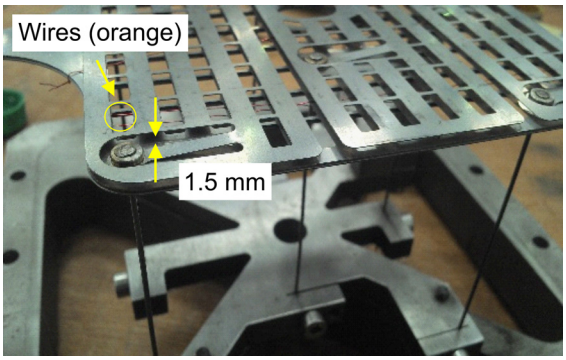

FIG. 11. Test 8. Excessive foil preloading.

seat, each upstand was split into two identical upstands to distribute reduced wear over a greater area of the foil. In addition, the upstands were receded by 0.5 mm towards the opening position, as can be seen in Fig. 10. The remaining two tests were carried out using this seat.

1. Test 8: Excessive preloading of foil flexures

With a new seat, motivated by the results of test 6, a 1.5 mm of preload was applied on the foil flexures to further improve the LS performance (Fig. 11). However, this amount of preload proved to be too much. It was impossible to move the valve freely over its full stroke length as the foil was locked in position by the upstands. Comparing the time domain signal with that of a free actuator also confirmed this (see Appendix D).

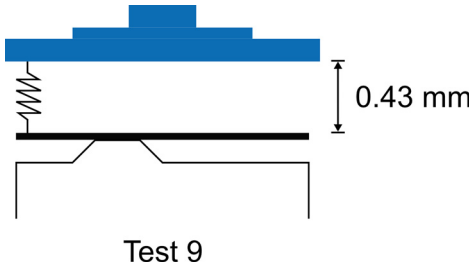

FIG. 12. Test 9. Valve configuration.

2. Test 9: Upstand recession

In the last test, the effect of upstand recession was investigated by reducing the amount of preload to 0.5 mm (Fig. 12). Instead of placing the wires, the foil was dimpled to provide necessary separation between the foil and the carrier. This test did not improve the valve performance. There was mediocre HS performance with a value of 32.4% of q_{max}, and relatively poor (but acceptable) LS performance with a $\theta_{c,min}$ of 30.1° aTDC. The HS performance was low, as it was not possible to reach the test engine limit; with the recessed upstands, the foil was guided short of the end of travel. The dimples may also have played a part in reducing the valve's ability to seal due to local distortions near the foil edges.

E. Valve wear and interstitial failure

Marks and damage to the foil were noticed during these tests and it therefore indicated that material wear may be a cause for concern. Figure 13 shows pictures of the valve foil used on the Mk.1 seat taken after several days of testing (~2 h total running).

It was revealed that the markings in the positions of the upstand plateaux are the products of wear between the foil and the upstands when in the semi-open position. The leading edge scoring is an evidence of two phenomena; one is the cam-guiding action which leads to improved HS performance, and second is the impact on valve opening which can be seen from the fluctuating curve in the valve motion trace (refer Fig. 17). Moreover, the interstitials failed on the edges on

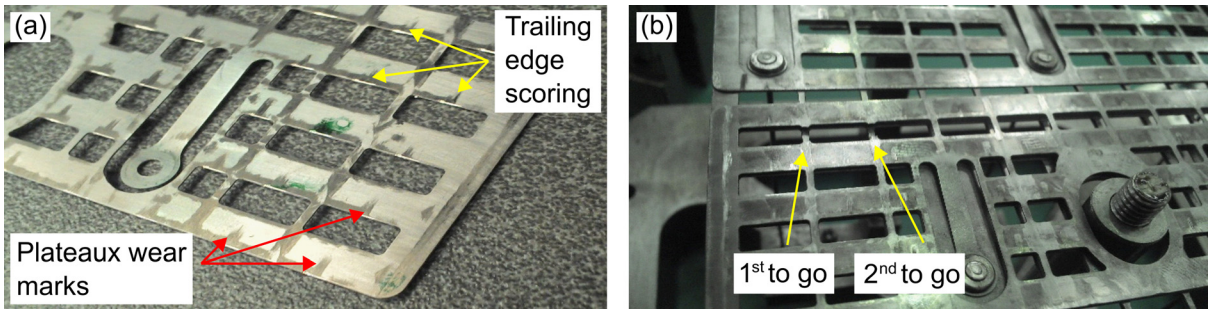

FIG. 13. Valve foil wear (a) and interstitial failure (b) after tests with the Mk.1 seat.

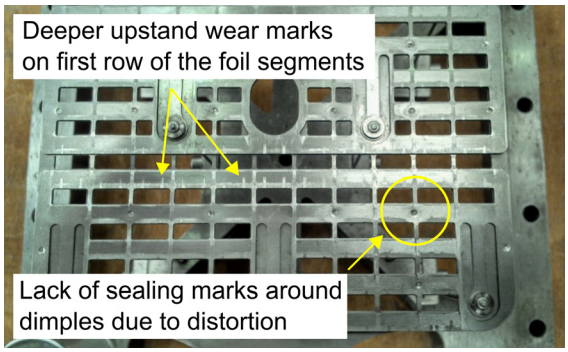

FIG. 14. Valve foil wear after tests with the Mk.2 seat.

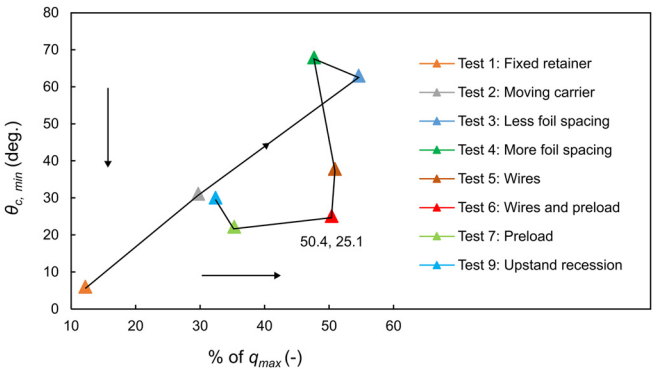

FIG. 15. Performance metrics and the optimal result (data point highlighted).

the leading side of the foil segments. The leading row of the interstitial supports of any valve segment experiences especially high loading, as the leading foil strip is cantilevered over the upstand edge. The middle strips, on the contrary, are supported at both ends, hence the loading is evenly distributed. Figure 13(b) reveals the interstitial failure occurring first at the side edge support and then moving to its inside ones.

The Mk.2 seat also resulted in wear marks (Fig. 14) and evidence of contact between the trailing foil edges and the upstands was found in the valve motion trace. It was not clear whether this wear was occurring during closure or opening, although the damage appeared to be wear rather than impact deformation, strongly suggesting that this was sliding wear during closure.

F. Test summary

The graph in Fig. 15 shows the development path expressed by the two performance metrics (high speed vs low speed). Moving from a retainer frame to a carrier frame design greatly improved the HS performance due to the shielding of the valve foil by the carrier, hence minimizing any chances of friction-locking. The introduction of upstand seat design made it possible to seal at even higher engine speeds, primarily due to the control of upforce/downforce on the foil during the cycle. However, this same shielding worsened the LS performance, as the valve could no longer close at small angles aTDC, resulting in more equivalent percentage loss in the piston stroke (which is undesirable). Foil flexure preload and the precise separation of the foil from the carrier by wires, dimples or etched carrier features, improved the LS performance without any outstanding loss in the HS performance. Excessive preloading disrupted the valve operation and hence it was not investigated further. Concerns about valve wear motivated the design of a seat with divided and receded upstands, but the HS performance suffered as the upstands could no longer force the foil into the correct closing position; the LS performance degraded with little margin comparatively. Table III summarizes the valve design modifications and the corresponding performance metrics.

VII. CONCLUDING REMARKS AND FUTURE RESEARCH

In this study, an improved design of a novel screen valve was presented by going through a series of tests conducted on a specially designed test engine. Two performance metrics were defined and the valve performance was evaluated for the case of a full-scale heat pump

TABLE III. Valve design modifications and performance summary.

	Valve modifications				Performance metrics	
Test	Type	Spacing (mm)	Wires Ø (mm)	Preload (mm)	% of maximum dynamic pressure	Minimum closure angle aTDC (°)
1	Retainer frame with a flat seat	0.5[a]	…	…	12.2	6.0
2	Carrier frame with a flat seat	0.5[a]	…	…	29.7	31.1
3	Carrier frame with the Mk.1 seat (central upstands)	0.11[b]	…	…	54.6	63.0
4		0.27[b]	…	…	47.7	67.9
5		0.27[b]	0.16	…	50.9	37.8
6		0.27[b]	0.16	∼1	50.4	25.1
7		0.27[b]	…	∼1	35.3	22.2
8	Carrier frame with the Mk.2 seat (receded upstands)	0.27[b]	0.16	1.5	No result	
9		0.27[b]	0.16	0.5	32.4	30.1

[a]Between the foil and seat.
[b]Between the foil and top of the upstand.

application. The novel features of the valve make it a good choice for use in reciprocating machines primarily in compressors, heat pump, and engine applications. Based on the results of this study, the improved design of this valve was implemented in the compressor–expander machine of a Pumped Heat Energy Storage (PHES) demonstrator system; this is the first system for grid-scale electrical energy storage and is located in Hampshire, UK. The system underwent commissioning recently and a separate study is being conducted which is expected to showcase the effect of the proposed valve in terms of the overall system performance. Besides thermodynamic benefits, the use of such a valve in any reciprocating machine for energy storage provides an economical option, as it ensures a compact design for the compressor and expander cylinders due to its ability to adjust within the cylinder head and piston. Moreover, with such valves, it becomes easier to switch between the compressor and expander modes quickly, as is required during charging and discharging modes of the storage cycle.

The experimental study was well supported by CFD analysis which has not been included in this paper due to space limitations. Based on the set criteria, the design used in test 6 presented the best results. However, good performance was achieved at the expense of wear effects which appeared high. During the research, several very difficult challenges were noticed alongside remarkable benefits. The main concern was the minimization of sliding contact of foil with the seat; the sliding of a thin, unlubricated sealing member (foil) must be eliminated or only permitted when there is very little load on the valve. This was partially addressed by the carrier frame and upstand seat design. Above all, the damping of valve motion is considered to be of critical importance to reduce acceleration stresses in the valve.

After positive results from this work, the authors are committed to address the issues of foil-upstand wear and valve damping in the next phase. Finally, it is suggested that the key observations which came out of this experimental investigation can prove to significantly overcome design challenges and open new avenues in valve designing trends. The key findings of this experimental study are mentioned below:

- Valve with a moving carrier seals at higher dynamic pressures than its retainer type counterpart. The retainer frame allows us to seal at smaller angles aTDC compared to the carrier design.
- The minimum closure angle ($\theta_{c,\ min}$) aTDC is independent of rotational speed as well as gas flow speed at constant density.
- Central upstands on the seat enable correct operation at high speeds, as they can guide the foil into the correct closing position. However, they result in poor performance at low speeds.
- Testing with the carrier frame and upstand seat design pushed the rig to its safe operating limit. However, the foil impacts the upstands during opening and closing events, leaving scoring and impact marks on the foil and the seat. At high speeds, the test engine friction-locks the foil, especially on the opening stroke upon flow reversal.
- Wires or dimples which separate the carrier from the foil can improve the LS performance. Likewise, a preload on the foil flexures shows potential improvement in similar performance. Wires or dimples offer no additional benefit if the foils are sufficiently preloaded although preload increases wear and damages the HS performance.
- With upstands, preloading can be applied to a specific limit beyond which the foil becomes stuck and valve operation is disrupted. Upstands receded by a certain distance no longer guide the valve into the correct closing position.
- Better HS and LS performances can be achieved at the cost of significant material wear.

ACKNOWLEDGMENTS

The authors wish to acknowledge the financial support provided by the Energy Technologies Institute (ETI), UK and the EPSRC (Engineering and Physical Sciences Research Council) through the Centre for Energy Systems Integration (No. EP/P001173/1) and Thermal Energy Challenge Network (No. EP/P005667/1).

APPENDIX A: HIGH SPEED METRICS

Technical specifications (Table II) and reference operating conditions (Table IV) observed in a full-scale heat pump have been used to calculate the maximum open port dynamic pressure

TABLE IV. Dynamic pressure ($q = \rho v^2$) under the maximum possible and actual operating conditions in a full-scale heat pump.[7]

	Maximum possible values				Under actual conditions			
	Compressor		Expander		Compressor		Expander	
Parameter	Inlet	Outlet	Inlet	Outlet	Inlet	Outlet	Inlet	Outlet
Pressure, P (bar)	1	12	12	1	1	12	12	1
Temperature, T (°C)	25	500	25	−160	25	500	25	−160
Density, ρ (kg m^{-3})	1.61	7.46	19.36	4.25	1.61	7.46	19.36	4.25
Closing angle, θ_c (°)	81.4	81.4	81.4	81.4	318.7	49.1	49.1	318.7
Piston velocity, v_p (m s^{-1})	5.30	5.30	5.30	5.30	−3.87	4.37	4.37	−3.87
Pore velocity, v_{pore} (m s^{-1})	26.5	26.5	26.5	26.5	−19.3	21.8	21.8	−19.3
Dynamic pressure, q_{pore} (kPa)	1.122	5.190	13.462[a]	2.958	0.597	3.522	9.136	1.574
% of $q_{max,\ pore}$ (–)	8.3	38.6	100.0	22.0	4.4	26.2	67.9	11.7

[a]Maximum value.

(13.462 kPa). The crank angle, θ, density of the flow, ρ, and the machine speed, N, are used to calculate the fluid dynamic pressure, q. The closing angle, θ_c, is used to determine the instantaneous velocity with respect to the crank angle, $ds/d\theta_c$. The angular speed, ω, is obtained by using $d\theta_c/dt = 2\pi N/60$. These two values can be multiplied to get the piston (or superficial flow) velocity, v_p. The valve porosity, σ, which is the ratio of the valve pore area, A_{pore}, to the cylinder bore area, A_p, can be used to evaluate v_{pore} using $\sigma = A_{pore}/A_p = v_p/v_{pore}$. The density of argon has been obtained by calling Refprop version 9.0 at the given state points.

It is noteworthy that, at constant rotational speed, the dynamic pressure of the flow through an open valve depends on the angle (and hence the piston speed) at which the valve closes around the cycle and the density of the flow. As shown in Table IV, the maximum possible dynamic pressure is obtained where the piston speed is maximum, theoretically this being at 81.4° aTDC. However, in reality, the valves either close at 49.1° or 318.7° aTDC; these are calculated using the ideal gas laws assuming adiabatic compression and expansion. Under actual conditions, the valve never closes at 81.4° aTDC. Therefore, the maximum operating dynamic pressure would be 67.9% of 13.462 kPa corresponding to a closing angle of 49.1° aTDC at the expander inlet.

APPENDIX B: LOW SPEED METRICS

At an earlier stage, few test runs were conducted to determine the relationship between the crank angle at the valve closure, θ_c, and the test engine speed, N. The results from this test and subsequent theoretical justification below provided the basis for establishing the low speed metrics (Sec. V B). The test resulted in an observation that when the valve foil was translated over the ports to the close position prior to the TDC, it would seal at approximately the same angle after the TDC ($\theta_c \approx 33.05°$) regardless of the machine speed, N (results from four runs are shown in Table V).

A simple theoretical explanation is provided here. A downward force, F, acting on mass, m, of the valve, is considered to be scaled with the dynamic pressure, $1/2\rho v^2$, of the passing gas (Fig. 16). The more the machine speed, N, the higher the rate of rotation, ω, but also the larger the downforce. These effects apparently cancel each other to reveal an expression [Eq. (B4)] that does not involve the flow speed. The downforce is given as

$$F \propto 1/2\rho v^2 A. \tag{B1}$$

The velocity can be related to the angular speed as

$$v \propto \omega \sin(\omega t) \cong \omega^2 t \,(\text{for small } \theta). \tag{B2}$$

TABLE V. Operating speed vs closing angle.

Test runs	N (rpm)	θ_c (°)
(i)	947.5	32.3
(ii)	1444.0	32.9
(iii)	1447.3	32.6
(iv)	1973.9	34.4

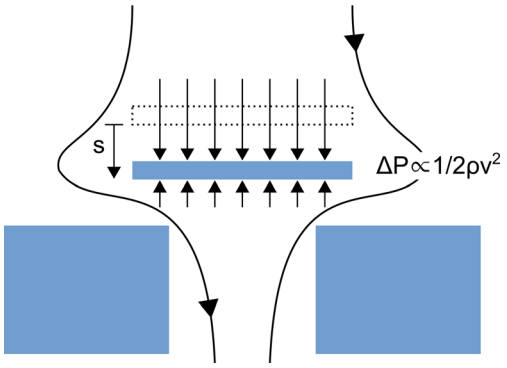

FIG. 16. Flow speed relationship with pressure difference.

Also knowing the acceleration (d^2s/dt^2), and substituting Eqs. (B1) and (B2) in Newton's second law ($F \propto ma$), we obtain Eq. (B3) as

$$1/2\rho\left(\omega^2 t\right)^2 A = m\left(d^2s/dt^2\right). \tag{B3}$$

Integrating the above expression twice with respect to time, and substituting the relationship ($\theta \propto \omega t$), results in the standalone crank angle, θ, on the left side as

$$\theta \propto (ms/A\rho)^{1/4}. \tag{B4}$$

This expression suggests that the crank angle is neither dependent on the flow speed, v, nor the machine speed, N.

APPENDIX C: VALVE MOTION EXPLAINED

Figure 17 shows the trace generated from the post-processing tool for a complete valve cycle comprising a closing and opening stroke. The sequence of events is highlighted on the figure using eight points. The rising edge of the valve control signal indicates the instant at which the actuator triggers the valve closure. The valve then commences its motion just a few degrees before TDC (1). It moves with a low constant speed as a result of frictional contact

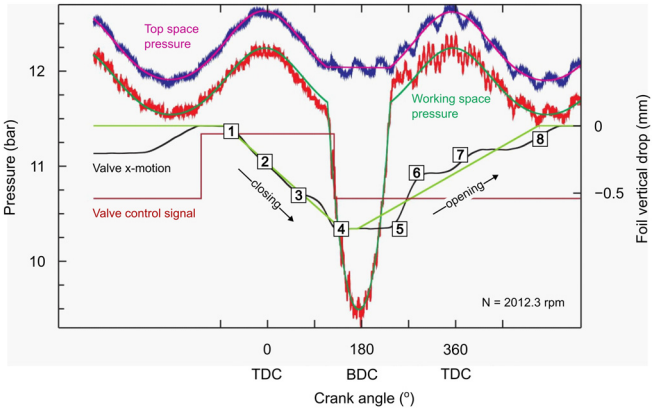

FIG. 17. Valve motion trace generated from the analysis program for a high speed run of test 3.

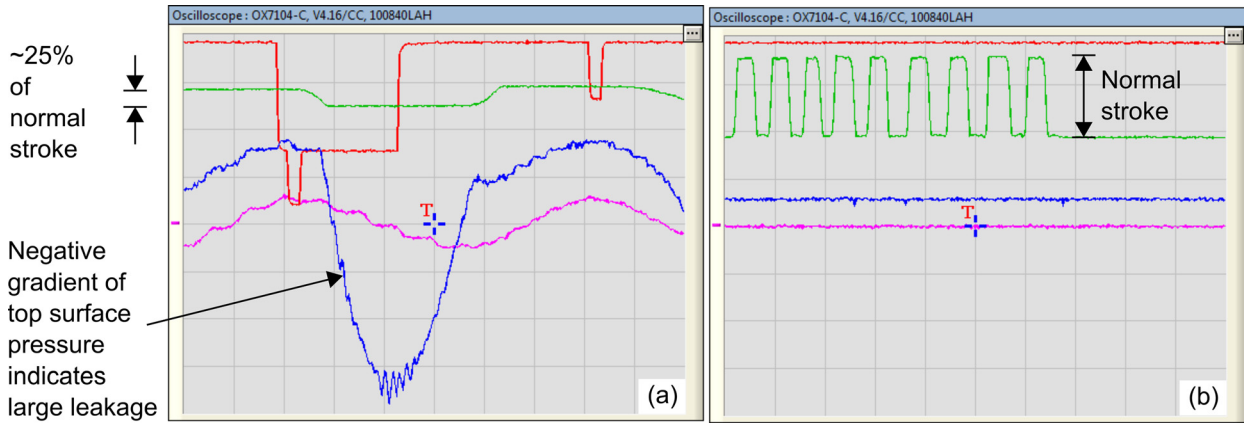

FIG. 18. Time domain signals showing reduced valve travel (a) when compared with the free actuator (b). Note that the signals from five sensors are shown in colors as: blue—top space pressure, magenta—working space pressure, red—TDC pulse (smaller amplitude) and cam pulse (larger amplitude), and green—valve displacement.

between the foil and the plateaux (1)–(3). After a deceleration due to an increase in the down force on the foil (3), the valve accelerates sharply to its closing position (4), this being the instant at which θ_c is recorded. This acceleration occurs when the foil passes over the edge of the upstand and slides down its slanted face.

After a dwell period (4) and (5), on opening, the valve accelerates quickly (5) as it is lifted from the seat via a reed valve action. It impacts the upstand and briefly stops (6) before continuing its translation at a lower speed. At the next TDC, the valve halts (7), as the flow through the valve reverses and the foil becomes friction-locked at the top of the upstand. Just prior to the next BDC, the valve recommences its motion (8), as the flow through the valve slows and the foil is eventually released from the friction-lock.

APPENDIX D: INCOMPLETE VALVE MOTION

Figure 18 shows a comparison of the time domain signals from test 8 with those obtained with a free valve movement. The green trace in Fig. 18(a) indicates that the valve did not move over the whole stroke. The top space pressure also leaked because of incomplete valve operation, as indicated by the blue trace.

DATA AVAILABILITY

Data supporting this publication are openly available under an Open Data Commons Open Database License. Additional metadata are available at doi:10.15128/r1fb494841, Ref. 34.

REFERENCES

[1]B. A. Taylor and T. O. McMahan, "Slide valve apparatus for internal combustion engine," U.S. patent 4,765,287 A (23/08/1988).
[2]K. Yazdi, "Internal combustion engine with sliding valves," U.S. patent 5,694,890 A (09/12/1997).
[3]C. W. Crall, "Sliding valve assembly," U.S. patent 8,360,395 B2 (29/01/2013).
[4]C. E. Price, "Valve apparatus for an internal combustion engine," U.S. patent 7,448,354 B2 (11/11/2008).
[5]F. A. Bowman and J. E. Briggs, "Slide-valve mechanism for engines," U.S. patent 1,123,986 A (05/01/1915).
[6]G. E. A. Hallett, "Slide valve engine," U.S. patent 1,922,678 A (15/08/1933).
[7]J. Howes, "Concept and development of a pumped heat electricity storage device," Proc. IEEE **100**, 493–503 (2012).
[8]See http://www.isentropic.co.uk/ for "National Facility for Pumped Heat Energy Storage Technologies" (last accessed 27 November, 2017).
[9]A. Smallbone, V. Jülch, R. Wardle, and A. P. Roskilly, "Levelised cost of storage for pumped heat energy storage in comparison with other energy storage technologies," Energy Convers. Manage. **152**, 221–228 (2017).
[10]K. Pichler, E. Lughofer, M. Pichler, T. Buchegger, E. P. Klement, and M. Huschenbett, "Fault detection in reciprocating compressor valves under varying load conditions," Mech. Syst. Signal Process. **70–71**, 104–119 (2016).
[11]F. Wang, G. Mu, and Q. Guo, "Design optimization of compressor reed valve based on axiomatic design," Int. J. Refrig. **72**, 132–139 (2016).
[12]L. R. Silva and C. J. Deschamps, "Modeling of gas leakage through compressor valves," Int. J. Refrig. **53**, 195–205 (2015).
[13]Y. Wang, C. Xue, X. Jia, and X. Peng, "Fault diagnosis of reciprocating compressor valve with the method integrating acoustic emission signal and simulated valve motion," Mech. Syst. Signal Process. **56-57**, 197–212 (2015).
[14]I. S. Hwang, S. J. Park, W. Oh, and Y. L. Lee, "Linear compressor discharge valve behavior using a rigid body valve model and a FSI valve model," Int. J. Refrig. **82**, 509–519 (2017).
[15]S. El Bouzidi, M. Hassan, and S. Ziada, "Experimental characterisation of the self-excited vibrations of spring-loaded valves," J. Fluids Struct. **76**, 558–572 (2018).
[16]M. Dalla Nora, T. D. M. Lanzanova, and H. Zhao, "Effects of valve timing, valve lift and exhaust backpressure on performance and gas exchanging of a two-stroke GDI engine with overhead valves," Energy Convers. Manage. **123**, 71–83 (2016).
[17]F. Lajus, C. Deschamps, and M. Alves, "Numerical analysis of seat impact of reed type valves," in 8th International Conference on Compressors and their Systems, London (2013).
[18]X. Yu, Y. Ren, Q. Tan, Z. Lu, X. Jia, and X. Wang, "Study on the torsional movement of a reed valve in a rotary compressor," Adv. Mech. Eng. **10**, 168781401877840 (2018).
[19]G. C. Rezende, E. Silva, and C. J. Deschamps, "Edge gap as a geometric parameter to characterize the sealing performance of compressor valves," Int. J. Refrig. **90**, 257–263 (2018).
[20]I. Zibani, R. Marumo, J. Chuma, and I. Ngebani, "Software controlled stepping valve system for a modern car engine," Proc. Manuf. **8**, 525–532 (2017).
[21]M. Dalla Nora and H. Zhao, "High load performance and combustion analysis of a four-valve direct injection gasoline engine running in the two-stroke cycle," Appl. Energy **159**, 117–131 (2015).
[22]Y. Zhang and H. Zhao, "Investigation of combustion, performance and emission characteristics of 2-stroke and 4-stroke spark ignition and CAI/HCCI operations in a DI gasoline," Appl. Energy **130**, 244–255 (2014).

[23]K. Brun, M. G. Nored, A. J. Smalley, and J. P. Platt, "Reciprocating compressor valve plate life and performance analysis," in Proceedings of 4th Conference of the EFRC, Antwerp, Belgium (2005).
[24]D. T. Branson, F. C. Wang, D. N. Johnston, D. G. Tilley, C. R. Bowen, and P. S. Keogh, "Piezoelectrically actuated hydraulic valve design for high bandwidth and flow performance," Proc. Inst. Mech. Eng., Part I **225**, 345–359 (2011).
[25]Y. Ma, Z. He, X. Peng, and Z. Xing, "Experimental investigation of the discharge valve dynamics in a reciprocating compressor for trans-critical CO_2 refrigeration cycle," Appl. Therm. Eng. **32**, 13–21 (2012).
[26]See https://www.uniquecarsandparts.com.au/how_it_works_valves for "Unique Cars and Parts. How it Works: Valves" (last accessed 25 June, 2018).
[27]See http://www.ekmpowershop2.com/ekmps/shops/readspeed/yamaha-aerox-reed-valve-2357-p.asp for "Readspeed: Reed Blocks" (last accessed 25 June, 2018).
[28]See https://www.cookcompression.com/products/compressor-valves/ring-damped-valve/ for "Cook Compression: Compressor Valves" (last accessed 25 June, 2018).
[29]J. S. Howes and J. Macnaghten, "Apparatus for use as a heat pump," European patent EP 1,872,069 B1 (17/11/ 2010).
[30]B. D. Morris, "Air conditioner," U.S. patent 5,295,370 A (22/03/1994).
[31]Y. Cengel and J. Cimbala, *Fluid Mechanics Fundamentals and Applications*, 3rd ed. (McGraw Hill Publication, New York, 2013).
[32]M. C. Albrecht, C. J. Nachtsheim, T. A. Albrecht, and R. D. Cook, "Experimental design for engineering dimensional analysis," Technometrics **55**, 257–270 (2013).
[33]The test engine employs five sensors to collect data; each sensor sends information (after amplification) to an oscilloscope, where it is shown as five voltage traces. See Sec. IV for more detail.
[34]A. Smallbone *et al.* (2017). "Levelised cost of storage data," Dataset http://dx.doi.org/10.17634/153224-1